Editors' Suggestion

Beyond Linear Response: Equivalence between Thermodynamic Geometry and Optimal Transport

Adrianne Zhong [1,2,*] and Michael R. DeWeese [1,2,3]

[1] *Department of Physics, University of California, Berkeley, Berkeley, California 94720, USA*
[2] *Redwood Center for Theoretical Neuroscience, University of California, Berkeley, Berkeley, California 94720, USA*
[3] *Department of Neuroscience, University of California, Berkeley, Berkeley, California 94720, USA*

(Received 2 April 2024; revised 14 June 2024; accepted 24 June 2024; published 31 July 2024)

A fundamental result of thermodynamic geometry is that the optimal, minimal-work protocol that drives a nonequilibrium system between two thermodynamic states in the slow-driving limit is given by a geodesic of the friction tensor, a Riemannian metric defined on control space. For overdamped dynamics in arbitrary dimensions, we demonstrate that thermodynamic geometry is equivalent to L^2 optimal transport geometry defined on the space of equilibrium distributions corresponding to the control parameters. We show that obtaining optimal protocols past the slow-driving or linear response regime is computationally tractable as the sum of a friction tensor geodesic and a counterdiabatic term related to the Fisher information metric. These geodesic-counterdiabatic optimal protocols are exact for parametric harmonic potentials, reproduce the surprising nonmonotonic behavior recently discovered in linearly biased double well optimal protocols, and explain the ubiquitous discontinuous jumps observed at the beginning and end times.

DOI: 10.1103/PhysRevLett.133.057102

Introduction—A consequence of the second law of thermodynamics is that finite-time processes require work to be irretrievably lost as dissipation. Recent studies in stochastic thermodynamics have aimed to characterize minimal-work protocols, which have applications for nanoscopic engineering [1–12] and for understanding biophysical systems [13–18]. In this Letter we unify disparate geometric approaches and arrive at a novel framework for obtaining and better understanding thermodynamically optimal protocols.

The problem statement is this: given a configuration space $x \in \mathbb{R}^d$, inverse temperature β, and potential energy function $U_\lambda(x)$ parametrized by $\lambda \in \mathcal{M}$, what is the optimal protocol $\lambda^*(t)$ connecting the parameter values λ_i and λ_f in a finite time τ that minimizes the work

$$W[\lambda(t)] = \int_0^\tau \frac{\mathrm{d}\lambda^\mu}{\mathrm{d}t} \left\langle \frac{\partial U_\lambda}{\partial \lambda^\mu} \right\rangle \mathrm{d}t? \tag{1}$$

Here, $\mathcal{M} \subseteq \mathbb{R}^n$ is an orientable m-dimensional manifold, locally resembling $\mathbb{R}^m$ everywhere with $m \leq n$. We use Greek indices to denote local coordinates of $\lambda \in \mathcal{M}$, and the Einstein summation convention (i.e., repeated Greek indices within a term are implicitly summed). The ensemble average $\langle \cdot \rangle$ is over trajectories $X(t)|_{t \in [0,\tau]}$ that start in equilibrium with λ_i and evolve via some specified Langevin dynamics under $U_{\lambda(t)}|_{t \in [0,\tau]}$.

Schmiedl and Seifert [19] showed that optimal protocols minimizing Eq. (1) have intriguing *discontinuous jumps* at the beginning and end times, which have proven to be ubiquitous [5,19–21,23–30]. Furthermore, optimal protocols can even be *nonmonotonic* in time [5,27].

Sivak and Crooks demonstrated through linear response [31] that in the slow-driving limit ($\tau \gg \tau_\mathrm{R}$, an appropriate relaxation timescale), optimal protocols are *geodesics* of a symmetric positive-definite [32] friction tensor defined in terms of equilibrium time-correlation functions. Treating the friction tensor as a Riemannian metric induces a geometric structure on the space of control parameters, known as "thermodynamic geometry." This approach is computationally tractable, as the friction tensor can be obtained through measurement, and geodesics on $\mathcal{M}$ can be determined by solving an ordinary differential equation. Geodesic protocols have been studied for a variety of systems including the Ising model [33–36], barrier crossing [15–17], bit erasure [2,37], and nanoscopic heat engines (after allowing temperature to be controlled) [9–12,38], but unfortunately their performance can degrade past the slow-driving regime [27].

Alternatively, when the ensemble of trajectories is additionally constrained to end in equilibrium with λ_f, finding the work-minimizing protocol for overdamped dynamics is equivalent to the Benamou-Brenier formulation of the L^2 optimal transport problem [39,40]—finding the dynamical mapping between the two distributions that has minimal integrated squared distance [41]—which itself yields a Riemannian-geometric structure [42–44]. The Benamou-Brenier solution is a time-dependent distribution and time-dependent velocity field that solves a continuity equation,

*Contact author: adrizhong@berkeley.edu

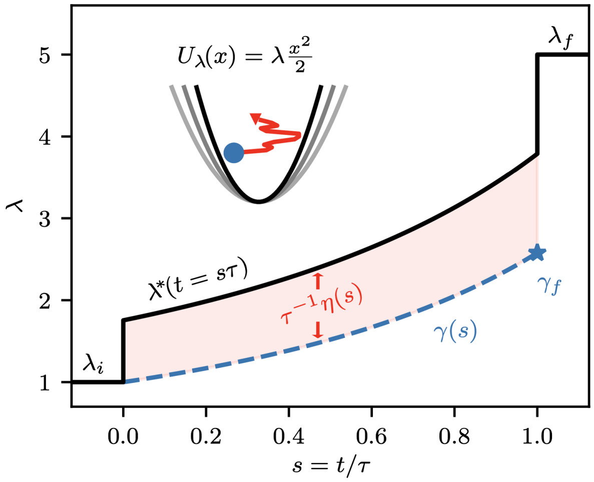

FIG. 1. Algorithm 1 reproduces the exact optimal protocol (black) for the variable-stiffness harmonic oscillator (depicted here, $\lambda_i = 1$, $\lambda_f = 5$, and $\tau = 0.5$) found in [19], as the sum of geodesic (dashed blue) and counterdiabatic (shaded red) components. The geodesic $\gamma(s)$ connects $\gamma(0) = \lambda_i$ to $\gamma(1) = \gamma_f$ (blue star) solving Eq. (21).

which in this Letter we explicitly identify as a desired probability density evolution and the additional counterdiabatic forcing needed to effectuate its faster-than-quasi-static time evolution (as studied in so-called engineered swift equilibration [45–47], counterdiabatic driving [48], and shortcuts to adiabaticity [49–57]). Remarkably, optimal protocols obtained in this manner are exact for arbitrary protocol durations τ [39]. Unfortunately, this approach involves solving coupled partial differential equations (PDEs) in configuration space ($\mathbb{R}^d$), which is typically infeasible for dimension $d \gtrsim 5$. Furthermore, the control space $\mathcal{M}$ must be sufficiently expressive in order to implement the optimal transport solution, which is often overly restrictive [58].

For overdamped dynamics in arbitrary dimension, [38] showed that the friction tensor may be obtained via a perturbative expansion of the Benamou-Brenier objective function. Here, we derive an even stronger result, that thermodynamic geometry is in fact *equivalent* to optimal transport geometry, in the sense that the friction tensor and the Benamou-Brenier problem restricted to equilibrium distributions parametrized by λ have identical geodesics and geodesic distances. Surprisingly, we find that a counterdiabatic component may be calculated using the Fisher information metric from information geometry [59–61]. We demonstrate that protocols obtained by adding this counterdiabatic term to thermodynamic geometry geodesics are analytically exact for parametric harmonic oscillators, reproduce recently discovered nonmonotonic behavior in certain optimal protocols [27], and satisfyingly explain the origin of jumps at beginning and end times.

Preliminaries—For each $\lambda \in \mathcal{M}$ there is a corresponding equilibrium distribution

$$\rho_\lambda^{\mathrm{eq}}(x) = \exp\{-\beta[U_\lambda(x) - F(\lambda)]\}, \tag{2}$$

where $F(\lambda) = -\beta^{-1} \ln \int \exp[-\beta U_\lambda(x')]\,\mathrm{d}x'$ is the equilibrium free energy of the potential energy $U_\lambda(\cdot)$. For ease of notation we will denote $\rho_i^{\mathrm{eq}} = \rho_{\lambda_i}^{\mathrm{eq}}$, $\rho_f^{\mathrm{eq}} = \rho_{\lambda_f}^{\mathrm{eq}}$, and $\Delta F = F(\lambda_f) - F(\lambda_i)$.

We consider overdamped Langevin equations, such that trajectories $X(t) \in \mathbb{R}^d$ follow the stochastic ODE

$$\mathrm{d}X(t) = -\nabla U_{\lambda(t)}(X(t))\,\mathrm{d}t + \sqrt{2\beta^{-1}}\mathrm{d}B(t), \tag{3}$$

where $B(t) \in \mathbb{R}^d$ is an instantiation of standard Brownian motion [62]. Here, we will consider only isothermal protocols, so without loss of generality we set $\beta = 1$.

The probability density $\rho(x, t)$ corresponding to Eq. (3) undergoes a time evolution expressible either as a Fokker-Planck equation or a continuity equation of a gradient field

$$\frac{\partial \rho}{\partial t} = \mathcal{L}_{\lambda(t)}\rho \quad \text{or} \quad \frac{\partial \rho}{\partial t} = \nabla \cdot (\rho \nabla \phi), \tag{4}$$

where $\mathcal{L}_\lambda$ is the Fokker-Planck operator [63]

$$\mathcal{L}_\lambda \rho = \nabla^2 \rho + \nabla \cdot (\rho \nabla U_\lambda), \tag{5}$$

while ϕ is a scalar field that depends on both ρ and λ

$$\phi(x, t) = \ln \rho(x, t) + U_{\lambda(t)}(x, t). \tag{6}$$

The adjoint operator $\mathcal{L}_\lambda^\dagger$ acts on a scalar field $\psi(x)$ via [64]

$$[\mathcal{L}_\lambda^\dagger \psi](x) = \rho_\lambda^{\mathrm{eq}}(x)^{-1} \nabla \cdot [\rho_\lambda^{\mathrm{eq}}(x) \nabla \psi(x)]. \tag{7}$$

Finally, $f_\mu(x) \coloneqq -\partial U_\lambda(x)/\partial \lambda^\mu$ is the conjugate force to λ^μ. The excess conjugate force is then

$$\delta f_\mu(x) = -\left[\frac{\partial U_\lambda(x)}{\partial \lambda^\mu} - \left\langle \frac{\partial U_\lambda}{\partial \lambda^\mu} \right\rangle_\lambda^{\mathrm{eq}}\right] = \frac{\partial \ln \rho_\lambda^{\mathrm{eq}}(x)}{\partial \lambda^\mu}. \tag{8}$$

Thermodynamic geometry—In the slow-driving limit, the excess work, defined as the work [Eq. (1)] minus the equilibrium free energy difference $W_{\mathrm{ex}} = W - \Delta F$, is [65]

$$W_{\mathrm{ex}}[\lambda(t)] \approx \int_0^\tau \frac{\mathrm{d}\lambda^\mu}{\mathrm{d}t} \frac{\mathrm{d}\lambda^\nu}{\mathrm{d}t} g_{\mu\nu}(\lambda(t))\,\mathrm{d}t, \tag{9}$$

where

$$g_{\mu\nu}(\lambda) = \int_0^\infty \langle \delta f_\mu(X(t')) \delta f_\nu(X(0)) \rangle_\lambda^{\mathrm{eq}}\,\mathrm{d}t' \tag{10}$$

is the symmetric positive-definite [32] friction tensor. Here, $\langle \cdot \rangle_\lambda^{\mathrm{eq}}$ denotes an equilibrium average (i.e., $X(0) \sim \rho_\lambda^{\mathrm{eq}}$, and trajectories undergo Langevin dynamics [Eq. (3)] with constant λ).

Remarkably, the friction tensor induces a Riemannian geometry on control space $(\mathcal{M}, g)$ known as "thermodynamic geometry," with squared thermodynamic length between $\lambda_A, \lambda_B \in \mathcal{M}$ given by minimizing the path action

$$\mathcal{T}^2(\lambda_A, \lambda_B) = \min_{\lambda(s)|_{s\in[0,1]}} \left\{ \int_0^1 \frac{\mathrm{d}\lambda^\mu}{\mathrm{d}s} \frac{\mathrm{d}\lambda^\nu}{\mathrm{d}s} g_{\mu\nu}(\lambda(s))\, \mathrm{d}s \,\middle|\, \text{satisfying } \lambda(0) = \lambda_A, \lambda(1) = \lambda_B \right\}. \tag{11}$$

In the slow-driving limit, optimal protocols $\lambda^*(t)$ connecting λ_i and λ_f in time τ are time-rescaled versions of geodesics of Eq. (11), and the optimal excess work scales inversely with protocol time $W_{\mathrm{ex}}^* \approx \mathcal{T}^2(\lambda_i, \lambda_f)/\tau$ [65,66].

While this geometric framework is both mathematically elegant and computationally tractable, geodesic protocols are fundamentally approximate; their performance often degrades for sufficiently small protocol times, in some cases performing even worse than a linear interpolation protocol [27].

Optimal transport geometry—Optimal transport is traditionally formulated as finding the transport map sending a distribution ρ_A to another ρ_B that minimizes an integrated (L^2) squared distance. This minimal integrated squared distance defines the squared L^2-Wasserstein metric distance between probability distributions, which was shown in [41] to also be the minimum of a path action

$$\mathcal{W}_2^2[\rho_A, \rho_B] = \min_{\rho_s, \phi_s|_{s\in[0,1]}} \left\{ \int_0^1 \int \rho_s(x) |\nabla \phi_s(x)|^2 \,\mathrm{d}x\, \mathrm{d}s \,\middle|\, \text{satisfying } \frac{\partial \rho_s}{\partial s} = \nabla \cdot (\rho_s \nabla \phi_s), \rho_0 = \rho_A, \rho_1 = \rho_B \right\}. \tag{12}$$

Here, $\rho_s(\cdot)|_{s\in[0,1]}$ is a trajectory of configuration space probability densities $\mathcal{P}(\mathbb{R}^d)$ [67], and $\phi_s(\cdot)|_{s\in[0,1]}$ is a trajectory of scalar fields that yield gradient velocity fields $v_s = -\nabla\phi_s$ satisfying the continuity equation $\partial_s \rho_s = -\nabla \cdot (\rho_s v_s)$ [68]. This so-called Benamou-Brenier formulation of optimal transport [Eq. (12)] reveals a Riemannian structure on the space of probability distributions known as Otto calculus [42–44]: on this manifold of probability distributions $M \coloneqq \mathcal{P}(\mathbb{R}^d)$, a "point" is a probability distribution $\rho \in M$, a "tangent space vector" is a gradient velocity field identifiable (up to a constant offset) by a scalar field $\phi \in T_\rho(M)$, and geodesics are the argmin of Eq. (12).

For overdamped dynamics, the work-minimizing protocol satisfying boundary conditions $\rho(\cdot, 0) = \rho_i^{\mathrm{eq}}$ and $\rho(\cdot, \tau) = \rho_f^{\mathrm{eq}}$ is a time-scaled solution of Eq. (12) for $\rho_A = \rho_i^{\mathrm{eq}}$, $\rho_B = \rho_f^{\mathrm{eq}}$, assuming sufficiently expressive control (described in the following paragraph) [39]. [See the Supplemental Material (SM) for a concise derivation [69].] From the continuity equation form of $\partial\rho(\cdot, t)/\partial t$ [Eqs. (4) and (6)], the optimal protocol $\lambda^*(t)$ for finite time τ can be expressed in terms of ρ_s^* and ϕ_s^* that solve Eq. (12), as satisfying (up to a constant offset)

$$U_{\lambda^*(t)}(x) = -\ln \rho_{t/\tau}^*(x) + \tau^{-1} \phi_{t/\tau}^*(x). \tag{13}$$

The first term corresponds to the Benamou-Brenier geodesic ρ_s^*, and the second one with ϕ_s^* is a counterdiabatic term that drives the probability distribution solving Eq. (4) to match the geodesic $\rho(\cdot, t) = \rho_{t/\tau}^*$ (see [72]).

Remarkably, this solution is *exact* for any finite τ, and it provides a geometric interpretation for these work-minimizing protocols as optimal transport geodesics connecting ρ_i^{eq} to ρ_f^{eq}. Through the time-scaling $t = \tau s$, it follows that $W_{\mathrm{ex}}^* = \mathcal{W}_2^2[\rho_i^{\mathrm{eq}}, \rho_f^{\mathrm{eq}}]/\tau$ is a *tight* lower bound for excess dissipation in this additionally constrained setting [74,75]. However, there are two important caveats to this approach: first, solving Eq. (12) involves PDEs on configuration space, which generally for dimension $d \gtrsim 5$ is computationally intractable (although, see [76–79] for sophisticated modern machine learning methods, as well as [58]). Second, the control parameters must be sufficiently expressive in the sense that for all $t \in (0, \tau)$ there has to be a $\lambda \in \mathcal{M}$ that satisfies Eq. (13). Worse yet, there might not be *any* admissible protocols that can satisfy the terminal constraint $\rho(\cdot, \tau) = \rho_f^{\mathrm{eq}}$ [58].

Without the terminal condition, this problem is no longer overconstrained. The optimal excess work can be expressed as a minimum over $\rho_f = \rho(\cdot, \tau)$ (see the SM [69]),

$$W_{\mathrm{ex}}^* = \min_{\rho_f} \mathcal{W}_2^2[\rho_i^{\mathrm{eq}}, \rho_f]/\tau + D_{\mathrm{KL}}(\rho_f | \rho_f^{\mathrm{eq}}), \tag{14}$$

where the additional KL-divergence cost

$$D_{\mathrm{KL}}(\rho_A | \rho_B) \coloneqq \int \rho_A(x) \ln \frac{\rho_A(x)}{\rho_B(x)} \mathrm{d}x \tag{15}$$

is the dissipation from the equilibration $\rho_f \to \rho_f^{\mathrm{eq}}$ that occurs for $t > \tau$ (see [80]). Optimal protocols $\lambda^*(t)$ are also obtained via Eqs. (12) and (13), but now with $\rho_A = \rho_i^{\mathrm{eq}}$ and $\rho_B = \rho_f^*$ that minimizes Eq. (14). Without the restrictive terminal constraint, protocols that approximate Eq. (13) are allowed (in the case of limited expressivity), and may be near-optimal in performance [29,34].

Demonstrating equivalence of geometries—We start by expressing Eq. (10) with the time propagator (e.g., see

Chapter 4.2 of [63])

$$g_{\mu\nu}(\lambda) = \int_0^\infty \int \rho_\lambda^{\mathrm{eq}}(x)\delta f_\mu(x) e^{\mathcal{L}_\lambda^\dagger t'} \delta f_\nu(x)\,\mathrm{d}x\,\mathrm{d}t'$$
$$= -\int \rho_\lambda^{\mathrm{eq}}(x)\delta f_\mu(x)\{\mathcal{L}_\lambda^\dagger\}^{-1}[\delta f_\nu](x)\,\mathrm{d}x. \qquad (16)$$

The second line comes from taking the time integral, where the inverse operator $\{\mathcal{L}_\lambda^\dagger\}^{-1}$ is defined in terms of a properly constructed Green's function [Eq. (40) in [84]]. This expression is the lowest order tensor found in a perturbative expansion of the Fokker-Planck equation [84].

By formally defining $\phi_\mu = \{\mathcal{L}_\lambda^\dagger\}^{-1}\delta f_\mu$ as (up to a constant offset) the scalar field solving $\mathcal{L}_\lambda^\dagger \phi_\mu = \delta f_\mu$, it is straightforward to show with Eqs. (7) and (8) that, for any protocol $\lambda(s)|_{s\in[0,1]}$,

$$\frac{\partial \rho_{\lambda(s)}^{\mathrm{eq}}}{\partial s} = \nabla\cdot(\rho_{\lambda(s)}^{\mathrm{eq}}\nabla\phi_s), \quad \text{where } \phi_s(x) = \frac{\mathrm{d}\lambda^\mu}{\mathrm{d}s}\phi_\mu(x). \quad (17)$$

Applying $\delta f_\mu = \mathcal{L}_\lambda^\dagger \phi_\mu$ and Eq. (7) to Eq. (16) shows that the thermodynamic distance [Eq. (11)] may be expressed as

$$\mathcal{T}^2(\lambda_A,\lambda_B) = \min_{\lambda(s),\phi_s|_{s\in[0,1]}} \left\{ \int_0^1 \int \rho_{\lambda(s)}^{\mathrm{eq}}(x)|\nabla\phi_s(x)|^2\,\mathrm{d}x\,\mathrm{d}s \,\middle|\, \text{satisfying } \frac{\partial\rho_{\lambda(s)}^{\mathrm{eq}}}{\partial s} = \nabla\cdot(\rho_{\lambda(s)}^{\mathrm{eq}}\nabla\phi_s), \lambda(0)=\lambda_A, \lambda(1)=\lambda_B \right\}. \quad (18)$$

This is our first major result: this expression is equivalent to the squared L^2-Wasserstein distance [Eq. (12)] with the constraint that $\rho_s|_{s\in[0,1]}$ is a trajectory of equilibrium distributions $\rho_{\lambda(s)}^{\mathrm{eq}}|_{s\in[0,1]}$. In other words, thermodynamic geometry induced by the friction tensor [Eq. (10)] on $\mathcal{M}$ is *equivalent* to optimal transport geometry restricted to the equilibrium distributions $\mathcal{P}_{\mathcal{M}}^{\mathrm{eq}}(\mathbb{R}^d)$ corresponding to $\mathcal{M}$ [85], and thus share the same geodesics and geodesic distances.

Up until now, thermodynamic geometry has prescribed optimal protocols as friction tensor geodesics joining λ_i and λ_f, which are approximate for finite τ. Optimal transport solutions require solving PDEs, but yield exact optimal protocols containing both geodesic and counterdiabatic components [Eq. (13)]. Our unification of geometries suggests that thermodynamic geometry protocols may be made exact by including a counterdiabatic term.

Geodesic-counterdiabatic optimal protocols—From here we consider the control-affine parametrization [86]

$$U_\lambda(x) = U_{\mathrm{fixed}}(x) + U_{\mathrm{offset}}(\lambda) + \lambda^\mu U_\mu(x), \qquad (19)$$

and control space $\lambda\in\mathcal{M}=\mathbb{R}^m$. It follows from the equivalence of thermodynamic and optimal transport geometries that the optimal protocol should have the form

$$\lambda^*(t) = \gamma(t/\tau) + \tau^{-1}\eta(t/\tau), \qquad (20)$$

namely the sum of a geodesic term and a counterdiabatic term that correspond to the two terms in Eq. (13), where $\rho_s^*|_{s\in[0,1]}$ and $\phi_s^*|_{s\in[0,1]}$ solve Eq. (12) with $\rho_A = \rho_i^{\mathrm{eq}}$ and $\rho_B = \rho_f^*$ from Eq. (14). Here, $\gamma(s)$ will be a geodesic of $g(\lambda)$ joining $\gamma(0)=\lambda_i$ to $\gamma(1)=\gamma_f$, where

$$\gamma_f = \arg\min_\lambda \mathcal{T}^2(\lambda_i,\lambda)/\tau + D_{\mathrm{KL}}(\rho_\lambda^{\mathrm{eq}}|\rho_f^{\mathrm{eq}}). \qquad (21)$$

We show in Appendix A that the counterdiabatic term is

$$\eta(s) = h^{-1}(\gamma(s))g(\gamma(s))\left[\frac{\mathrm{d}\gamma(s)}{\mathrm{d}s}\right], \qquad (22)$$

where, intriguingly, h is the Fisher information metric [87]

$$h_{\mu\nu}(\lambda) = \int \rho_\lambda^{\mathrm{eq}}(x)\delta f_\mu(x)\delta f_\nu(x)\,\mathrm{d}x, \qquad (23)$$

which also induces a Riemannian geometry on the space of parametric equilibrium probability distributions $(\mathcal{M},h)$ known as "information geometry" [59–61]. Equation (22) is exact in cases of sufficient expressivity [i.e., when Eq. (13) can be satisfied]; otherwise, $\eta(s)$ is the full solution projected onto $\mathcal{M}$.

This is our second major result: the equivalence between thermodynamic and optimal transport geometries implies that optimal protocols beyond linear response require counterdiabatic forcing, and can be obtained for control-affine potentials [Eq. (19)] [88] via the following:

Algorithm 1. Geodesic-counterdiabatic opt. protocols for control-affine potentials [Eq. (19)].

Input: λ_i, λ_f, protocol time τ, metrics $g_{\mu\nu}(\lambda)$, $h_{\mu\nu}(\lambda)$ [Eqs. (10), (23)], KL divergence $D_{\mathrm{KL}}(\cdot|\rho_f^{\mathrm{eq}})$ [Eq. (15)].
1: Solve geodesic $\gamma(s)|_{s\in[0,1]}$ connecting $\gamma(0)=\lambda_i$ and $\gamma(1)=\gamma_f$ [obtained from Eq. (21)] under $g_{\mu\nu}$.
2: Calculate counterdiabatic term $\eta(s) = h^{-1}g[\mathrm{d}\gamma/\mathrm{d}s]$.
3: Return optimal protocol $\lambda^*(t) = \gamma(t/\tau) + \tau^{-1}\eta(t/\tau)$.

We emphasize that this procedure does not require solving any configuration-space PDEs. Moreover, in the limit $\tau \to \infty$, the counterdiabatic component in Eq. (20) vanishes and Eq. (21) is solved by $\gamma_f = \lambda_f$, and thus geodesic protocols from thermodynamic geometry are reproduced.

Examples—We show in Appendix B that Algorithm 1 reproduces exact optimal protocols solved in [19] for controlling a parametric harmonic potential. Figure 1 illustrates an optimal protocol for $U_\lambda(x) = \lambda x^2/2$. Notice that at $t = 0$ the counterdiabatic term is suddenly turned on, while at $t = \tau$ the geodesic ends at $\gamma_f \neq \lambda_f$ and the counterdiabatic term is suddenly turned off. Seen in this light, the discontinuous jumps in optimal protocols $\lambda^*(t)$ arise from the sudden turning on and off of counterdiabatic forcing, and the discontinuity of the geodesic at $t = \tau$. We note that starting in equilibrium at $t = 0$ and suddenly ending control at $t = \tau$ are both unnatural in biological settings; these generic discontinuous jumps can be seen as artifacts of the imposed boundary conditions.

Surprisingly, *nonmonotonic* optimal protocols have been found for the linearly biased double well [27]

$$U_\lambda(x) = E_0[(x^2 - 1)^2/4 - \lambda x], \tag{24}$$

for certain values of E_0 and τ [e.g., $\tau = 0.2$ in Fig. 2(a) for $E_0 = 16$]. Figure 2(b) illustrates protocols numerically obtained from Algorithm 1 (details given in the SM [69]). Because of the limited expressivity of the controls, these protocols are not identical to the exact optimal protocols obtained by solving PDEs [27] [Fig. 2(a)]. However, they reproduce significant properties (e.g., discontinuous jumps and nonmonotonicity, becoming exact in $\tau \to 0$ and $\tau \to \infty$), and lead to improved performance over geodesic protocols [Fig. 2(c)]. Figure 2(d) illustrates the nonmonotonic $\tau = 1$ protocol as a sum of geodesic and counterdiabatic terms. The tensors g and h [Fig. 2(e)] yield necessarily monotonic geodesics [Fig. 2(f)], and nonmonotonic counterdiabatic forcing [Fig. 2(g)] that leads to nonmonotonic optimal protocols.

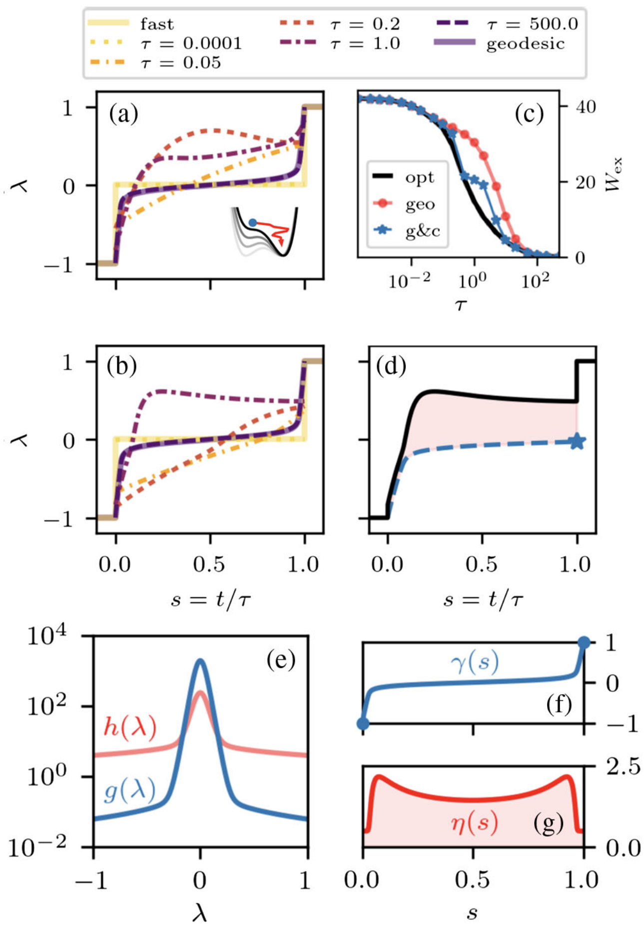

FIG. 2. (a) Exact optimal protocols obtained in [27] from solving PDEs, for the linearly biased double well [Eq. (24); $E_0 = 16$] for different protocol durations τ including the fast protocol $\tau \to 0$ [26] (solid yellow) and the friction tensor geodesic protocol (dark purple). (b) Geodesic-counterdiabatic protocols numerically obtained from Algorithm 1. (c) Geodesic-counterdiabatic protocols (blue stars) outperform the geodesic protocol (red circles) for all τ; cf. performance of exact optimal protocols (black). We examine the reduction in performance at $\tau \sim 2$ in the SM [69]. (d) The $\tau = 1$ protocol numerically obtained via Algorithm 1 (here $\gamma_f = 0.0291$), same coloring as Fig. 1. (e) The friction and Fisher information tensors yield (f) the geodesic $\gamma(s)$ (here $\lambda_A = -1$, $\lambda_B = 1$) and (g) the nonmonotonic counterdiabatic forcing $\eta(s)$.

Discussion—We have demonstrated the equivalence between overdamped thermodynamic geometry on $\mathcal{M}$—previously seen as an approximate framework—and L^2 optimal transport geometry on equilibrium distributions $\mathcal{P}^{\text{eq}}_{\mathcal{M}}(\mathbb{R}^d) \subset \mathcal{P}(\mathbb{R}^d)$. The resulting geodesic-counterdiabatic optimal protocols from Algorithm 1 are exact for parametric harmonic traps, and explain both the ubiquitous discontinuous jumps and the nonmonotonic behavior observed in optimal protocols.

We note that [57] presents a geodesic-counterdiabatic PDEs approach for underdamped dynamics. Additionally, underdamped optimal control has recently been related to a modified optimal transport problem [89,90]. We expect that the metric tensor in [57], the friction tensor [Eq. (10)] for underdamped dynamics [66], and the optimal transport specified in [89,90] may also be geometrically unified through methods similar to ours.

An interesting future direction will be to apply our findings to heat engines [9–12,38] and active matter systems [18,91], which have been studied with approximate geodesic protocols. We hope that the insight that minimal-work protocols require both geodesic and counterdiabatic components will prove to be useful in understanding the cyclic and fundamentally nonequilibrium processes that occur in biological systems.

Acknowledgments—This work greatly benefited from conversations with Adam Frim. A. Z. was supported by the Department of Defense (DOD) through the National Defense Science and Engineering Graduate (NDSEG) Fellowship Program. M. R. D. thanks Steve Strong and Fenrir LLC for supporting this project. This work was supported in part by the U.S. Army Research Laboratory and the U.S. Army Research Office under Contract No. W911NF-20-1-0151.

[1] G. Diana, G. B. Bagci, and M. Esposito, Phys. Rev. E **87**, 012111 (2013).
[2] P. R. Zulkowski and M. R. DeWeese, Phys. Rev. E **89**, 052140 (2014).
[3] K. Proesmans, J. Ehrich, and J. Bechhoefer, Phys. Rev. Lett. **125**, 100602 (2020).
[4] K. Proesmans, J. Ehrich, and J. Bechhoefer, Phys. Rev. E **102**, 032105 (2020).
[5] S. Whitelam, Phys. Rev. E **108**, 044138 (2023).
[6] T. Schmiedl and U. Seifert, Europhys. Lett. **81**, 20003 (2007).
[7] I. A. Martínez, É. Roldán, L. Dinis, and R. A. Rica, Soft Matter **13**, 22 (2017).
[8] D. Martin, C. Nardini, M. E. Cates, and É. Fodor, Europhys. Lett. **121**, 60005 (2018).
[9] P. Abiuso and M. Perarnau-Llobet, Phys. Rev. Lett. **124**, 110606 (2020).
[10] K. Brandner and K. Saito, Phys. Rev. Lett. **124**, 040602 (2020).
[11] A. G. Frim and M. R. DeWeese, Phys. Rev. E **105**, L052103 (2022).
[12] A. G. Frim and M. R. DeWeese, Phys. Rev. Lett. **128**, 230601 (2022).
[13] P. Geiger and C. Dellago, Phys. Rev. E **81**, 021127 (2010).
[14] C. Dellago and G. Hummer, Entropy **16**, 41 (2013).
[15] D. A. Sivak and G. E. Crooks, Phys. Rev. E **94**, 052106 (2016).
[16] J. N. E. Lucero, A. Mehdizadeh, and D. A. Sivak, Phys. Rev. E **99**, 012119 (2019).
[17] S. Blaber and D. A. Sivak, Europhys. Lett. **139**, 17001 (2022).
[18] L. K. Davis, K. Proesmans, and É. Fodor, Phys. Rev. X **14**, 011012 (2024).
[19] T. Schmiedl and U. Seifert, Phys. Rev. Lett. **98**, 108301 (2007).
[20] The discontinuities in the protocol are also taken into account in the integral Eq. (1).
[21] Gomez-Marin *et al*. found that optimal protocols for underdamped dynamics have even worse regularity [22]; at starting and end times, they have Dirac impulses!.
[22] A. Gomez-Marin, T. Schmiedl, and U. Seifert, J. Chem. Phys. **129** (2008).
[23] H. Then and A. Engel, Phys. Rev. E **77**, 041105 (2008).
[24] M. V. S. Bonança and S. Deffner, Phys. Rev. E **98**, 042103 (2018).
[25] P. Nazé, S. Deffner, and M. V. Bonança, J. Phys. Commun. **6**, 083001 (2022).
[26] S. Blaber, M. D. Louwerse, and D. A. Sivak, Phys. Rev. E **104**, L022101 (2021).
[27] A. Zhong and M. R. DeWeese, Phys. Rev. E **106**, 044135 (2022).
[28] A. Rolandi, M. Perarnau-Llobet, and H. J. Miller, New J. Phys. **25**, 073005 (2023).
[29] M. C. Engel, J. A. Smith, and M. P. Brenner, Phys. Rev. X **13**, 041032 (2023).
[30] M. Esposito, R. Kawai, K. Lindenberg, and C. Van den Broeck, Europhys. Lett. **89**, 20003 (2010).
[31] R. Zwanzig, *Nonequilibrium Statistical Mechanics* (Oxford University Press, New York, 2001).
[32] We assume the parametrization of U_λ is such that $\rho_\lambda^{\mathrm{eq}}$ are different for different λ; otherwise, the tensor could be semipositive definite.
[33] G. M. Rotskoff and G. E. Crooks, Phys. Rev. E **92**, 060102(R) (2015).
[34] T. R. Gingrich, G. M. Rotskoff, G. E. Crooks, and P. L. Geissler, Proc. Natl. Acad. Sci. U.S.A. **113**, 10263 (2016).
[35] G. M. Rotskoff, G. E. Crooks, and E. Vanden-Eijnden, Phys. Rev. E **95**, 012148 (2017).
[36] M. D. Louwerse and D. A. Sivak, J. Chem. Phys. **156** (2022).
[37] M. Scandi, D. Barker, S. Lehmann, K. A. Dick, V. F. Maisi, and M. Perarnau-Llobet, Phys. Rev. Lett. **129**, 270601 (2022).
[38] S. Chennakesavalu and G. M. Rotskoff, Phys. Rev. Lett. **130**, 107101 (2023).
[39] E. Aurell, C. Mejía-Monasterio, and P. Muratore-Ginanneschi, Phys. Rev. Lett. **106**, 250601 (2011).
[40] S. Ito, Inf. Geom. **7**, 441 (2024).
[41] J.-D. Benamou and Y. Brenier, Numer. Math. **84**, 375 (2000).
[42] F. Otto, *The geometry of dissipative evolution equations: the porous medium equation* (Taylor & Francis, 2001), 10.1081/PDE-100002243.
[43] P. Kniefacz, Otto calculus or the weak Riemannian strucutre of $(\mathcal{P}_2(M), \mathcal{W}_2)$, Ph.D. thesis, Technische Universität Wien, 2017.
[44] C. Villani, *Topics in Optimal Transportation* (American Mathematical Soc., Providence, 2021), Vol. 58, see Ch. 8.
[45] I. A. Martínez, A. Petrosyan, D. Guéry-Odelin, E. Trizac, and S. Ciliberto, Nat. Phys. **12**, 843 (2016).
[46] A. Baldassarri, A. Puglisi, and L. Sesta, Phys. Rev. E **102**, 030105(R) (2020).
[47] A. G. Frim, A. Zhong, S.-F. Chen, D. Mandal, and M. R. DeWeese, Phys. Rev. E **103**, L030102 (2021).
[48] S. Iram, E. Dolson, J. Chiel, J. Pelesko, N. Krishnan, Ö. Güngör, B. Kuznets-Speck, S. Deffner, E. Ilker, J. G. Scott *et al.*, Nat. Phys. **17**, 135 (2021).
[49] E. Torrontegui, S. Ibáñez, S. Martínez-Garaot, M. Modugno, A. del Campo, D. Guéry-Odelin, A. Ruschhaupt, X. Chen, and J. G. Muga, in *Advances in Atomic, Molecular, and Optical Physics* (Elsevier, New York, 2013), Vol. 62, pp. 117–169.
[50] C. Jarzynski, Phys. Rev. A **88**, 040101(R) (2013).
[51] S. Campbell and S. Deffner, Phys. Rev. Lett. **118**, 100601 (2017).
[52] D. Guéry-Odelin, A. Ruschhaupt, A. Kiely, E. Torrontegui, S. Martínez-Garaot, and J. G. Muga, Rev. Mod. Phys. **91**, 045001 (2019).

[53] C. A. Plata, A. Prados, E. Trizac, and D. Guéry-Odelin, Phys. Rev. Lett. **127**, 190605 (2021).
[54] D. Guéry-Odelin, C. Jarzynski, C. A. Plata, A. Prados, and E. Trizac, Rep. Prog. Phys. **86**, 035902 (2023).
[55] A. Patra and C. Jarzynski, Phys. Rev. Res. **3**, 013087 (2021).
[56] G. Li, H. T. Quan, and Z. C. Tu, Phys. Rev. E **96**, 012144 (2017).
[57] G. Li, J.-F. Chen, C. P. Sun, and H. Dong, Phys. Rev. Lett. **128**, 230603 (2022).
[58] J. Klinger and G. M. Rotskoff, arXiv:2402.17931.
[59] R. A. Fisher, Phil. Trans. R. Soc. A **222**, 309 (1922).
[60] C. R. Rao, in *Breakthroughs in Statistics: Foundations and Basic Theory* (Springer, New York, 1992), pp. 235–247.
[61] S.-i. Amari, *Information Geometry and its Applications* (Springer, New York, 2016), Vol. 194.
[62] B. Oksendal, *Stochastic Differential Equations: An Introduction with Applications* (Springer Science & Business Media, New York, 2013).
[63] H. Risken and H. Risken, *Fokker-Planck Equation* (Springer, New York, 1996).
[64] The operator $\mathcal{L}_\lambda^\dagger$ is also known as the backward Kolmogorov operator or the "generator" of Eq. (3). By substituting in Eq. (2) into Eq. (7), one readily recovers the perhaps more familiar expression $\mathcal{L}_\lambda^\dagger \psi = \nabla^2\psi - \nabla U_\lambda \cdot \nabla\psi$ [63].
[65] D. A. Sivak and G. E. Crooks, Phys. Rev. Lett. **108**, 190602 (2012).
[66] P. R. Zulkowski, D. A. Sivak, G. E. Crooks, and M. R. DeWeese, Phys. Rev. E **86**, 041148 (2012).
[67] For technical reasons, each probability distribution must have finite second moment [44].
[68] In the original formulation the optimization is over trajectories of effective vector fields $v_s|_{s\in[0,1]}$ as opposed to scalar fields $\phi_s|_{s\in[0,1]}$ [41]; however, it is straightforward to prove that under optimality, each v_s must be a gradient field [40,41].
[69] See Supplemental Material at http://link.aps.org/supplemental/10.1103/PhysRevLett.133.057102, which includes Refs. [70,71], for additional information about the optimal transport formulation of optimal protocols, and numerical methods used to study the linearly biased double well.
[70] V. Holubec, K. Kroy, and S. Steffenoni, Phys. Rev. E **99**, 032117 (2019).
[71] G. E. Crooks, Phys. Rev. Lett. **99**, 100602 (2007).
[72] Note that the two terms $-\ln\rho_s^*$ and ϕ_s^* corresponding exactly to time-reversal-symmetric $U_0(\cdot,t)$ and time-reversal-asymmetric $U_1(\cdot,t)$ found in Eqs. (6)–(8) in [56] and Eq. (8) in [73]; also, see Eq. (6) in [4] and Eq. (2) in the SM of [45] for dimension $d=1$.
[73] A. Zhong, B. Kuznets-Speck, and M. R. DeWeese, arXiv:2304.12287.
[74] A. Dechant and Y. Sakurai, arXiv:1912.08405.
[75] M. Nakazato and S. Ito, Phys. Rev. Res. **3**, 043093 (2021).
[76] C. Beck, S. Becker, P. Grohs, N. Jaafari, and A. Jentzen, J. Sci. Comput. **88**, 1 (2021).
[77] J. Han, A. Jentzen, and W. E, Proc. Natl. Acad. Sci. U.S.A. **115**, 8505 (2018).
[78] Y. Chen, B. Hosseini, H. Owhadi, and A. M. Stuart, J. Comput. Phys. **447**, 110668 (2021).
[79] M. S. Albergo, N. M. Boffi, and E. Vanden-Eijnden, arXiv:2303.08797.
[80] Interestingly, this cost function is equivalent to the celebrated Jordan-Kinderlehrer-Otto scheme used to study convergence properties of the Fokker-Planck equation [81], as observed in [82], with effective time step $h=\tau/2$. We study the time scaling of these unconstrained-end-state optimal protocols in a separate upcoming work [83].
[81] R. Jordan, D. Kinderlehrer, and F. Otto, SIAM J. Math. Anal. **29**, 1 (1998).
[82] Y. Chen, T. T. Georgiou, and A. Tannenbaum, IEEE Trans. Autom. Control **65**, 2979 (2019).
[83] A. Zhong and M. R. DeWeese (unpublished).
[84] N. S. Wadia, R. V. Zarcone, and M. R. DeWeese, Phys. Rev. E **105**, 034130 (2022).
[85] This is entirely analogous to how both the unit ball $B^2 = \{(x,y,z)|x^2+y^2+z^2\le 1\}$ and unit sphere $S^2 = \{(x,y,z)|x^2+y^2+z^2=1\}$ can be seen as submanifolds of Euclidean space $\mathbb{R}^3$; while geodesics connecting two points in the unit ball are equivalent to straight-line Euclidean geodesics, on the unit sphere they differ.
[86] The term $U_{\mathrm{offset}}(\lambda)$ is constant in x so that $\nabla U_{\mathrm{offset}}=0$, but is allowed to be nonlinear in λ. It is necessary to express certain potentials, e.g., the variable center harmonic trap $U_\lambda(x) = (x-\lambda)^2/2 = x^2/2 + \lambda^2/2 - \lambda x$.
[87] Traditionally the Fisher information metric is denoted as $h_{\mu\nu}(\lambda) = \int \rho_\lambda^{\mathrm{eq}}(\partial \ln\rho_\lambda^{\mathrm{eq}}/\partial\lambda^\mu)(\partial\ln\rho_\lambda^{\mathrm{eq}}/\partial\lambda^\nu)\,\mathrm{d}x$ [which can be seen as equivalent via Eq. (8)].
[88] In the event that the potential energy U_λ may not be expressed in control-affine form [Eq. (19)], the construction of the counterdiabatic term is still valid, granted that for all $s\in[0,1]$ the potential energy is locally linearizable around $\lambda=\gamma(s)$, and the magnitude of the resulting $\eta(s)$ is small enough so that the local linearization is a good approximation.
[89] R. Sabbagh, O. M. Miangolarra, and T. T. Georgiou, arXiv:2312.07788.
[90] J. Sanders, M. Baldovin, and P. Muratore-Ginanneschi, arXiv:2403.00679.
[91] P. R. Zulkowski, D. A. Sivak, and M. R. DeWeese, PLoS One **8**, e82754 (2013).
[92] G. Khan and J. Zhang, Inf. Geom. **5**, 47 (2022).
[93] One may choose other projection operators to act on Eq. (A2), but then nonconventional tensors would have to be defined. Furthermore, the particular interpretation for Eq. (A4), that the geometries associated with g and h convert between horizontal and vertical displacements, will be lost.
[94] bayerj (https://stats.stackexchange.com/users/2860/bayerj), KL divergence between two univariate Gaussians, Cross Validated, https://stats.stackexchange.com/q/7440 (version: 2022-12-27), https://stats.stackexchange.com/q/7440.

End Matter

Appendix A: Counterdiabatic driving expression—In this appendix we derive our expression for the counterdiabatic term [Eq. (22)]. Per definition, the counterdiabatic term $\phi_s(x) = \eta^\mu(s)U_\mu(x)$ is constructed to solve the continuity equation

$$\frac{\partial\rho^{\text{eq}}_{\gamma(s)}}{\partial s}(x) = \nabla\cdot[\rho^{\text{eq}}_{\gamma(s)}(x)\nabla\phi_s(x)]. \qquad \text{(A1)}$$

We can divide by $\rho^{\text{eq}}_\lambda(x)$ and plug in $\partial_s \ln\rho^{\text{eq}}_{\gamma(s)} = [\mathrm{d}\gamma(s)/\mathrm{d}s]\delta f_\mu(x)$ to obtain

$$\frac{\mathrm{d}\gamma^\mu}{\mathrm{d}s}\delta f_\mu(x) = -\eta^\nu(s)[\mathcal{L}^\dagger_{\gamma(s)}\delta f_\nu](x), \qquad \text{(A2)}$$

where we have used the fact that $U_\nu(x) = -\delta f_\nu + \text{const}$, and that the adjoint operator [Eq. (7)] satisfies $\mathcal{L}^\dagger_\lambda[\psi + c] = \mathcal{L}^\dagger_\lambda[\psi]$ for any scalar field $\psi(x)$ and constant $c \in \mathbb{R}$.

Because of the limited expressivity of available controls in a given problem, it might not be possible to satisfy Eq. (A2). However, this potential insolubility is resolved by applying a projection operator to both sides

$$\frac{\mathrm{d}\gamma^\mu}{\mathrm{d}s}\int\left[-\rho^{\text{eq}}_{\gamma(s)}(x)\delta f_\alpha(x)\{\mathcal{L}^\dagger_{\gamma(s)}\}^{-1}\right]\delta f_\mu(x)\,\mathrm{d}x = -\eta^\nu(s)\int\left[-\rho^{\text{eq}}_{\gamma(s)}(x)\delta f_\alpha(x)\{\mathcal{L}^\dagger_{\gamma(s)}\}^{-1}\right][\mathcal{L}^\dagger_{\gamma(s)}\delta f_\nu](x)\,\mathrm{d}x, \qquad \text{(A3)}$$

which yields

$$g_{\alpha\mu}(\gamma(s))\left[\frac{\mathrm{d}\gamma^\mu}{\mathrm{d}s}\right] = h_{\alpha\nu}(\gamma(s))\eta^\nu(s), \qquad \text{(A4)}$$

using the friction tensor and Fisher information metric expressions Eq. (16) and Eq. (23). Optimal transport geometry measures "horizontal" displacement while information geometry measures "vertical" displacement [92], so g and h can be seen to give the conversion between the left and right hand sides of Eq. (A1) [93].

Because the Fisher information metric is symmetric and positive-definite (assuming [32]), we can apply its inverse to Eq. (A4), thus reproducing Eq. (22).

Appendix B: Analytic reproduction of harmonic oscillator optimal protocols—In this appendix we show that Algorithm 1 exactly reproduces the optimal protocols for harmonic potentials first found in [19].

We first consider a variable-center harmonic potential in one dimension $U_\lambda(x) = (x-\lambda)^2/2$, both the friction and Fisher information tensors are spatially constant $g(\lambda) = f(\lambda) = 1$ due to translation symmetry. For any λ_f, the KL divergence is given by $D_{\text{KL}}(\rho^{\text{eq}}_\lambda|\rho^{\text{eq}}_f) = \int\rho^{\text{eq}}_\lambda(x)\ln[\rho^{\text{eq}}_\lambda(x)/\rho^{\text{eq}}_f(x)]\,\mathrm{d}x = (\lambda-\lambda_f)^2/2$, while the squared thermodynamic length is given by $\mathcal{T}^2(\lambda_i,\lambda) = (\lambda-\lambda_i)^2$. Without loss of generality we fix $\lambda_i = 0$. Following Algorithm 1, we obtain $\gamma_f = (1+2/\tau)^{-1}\lambda_f$ with geodesic $\gamma(s) = s\gamma_f$, and $\eta(s) = \gamma_f$. Ultimately, this yields the optimal protocol

$$\lambda^*(t) = \underbrace{[\lambda_f/(2+\tau)]t}_{\text{geodesic}} + \underbrace{1/(2+\tau)}_{\text{counterdiabatic}}, \quad \text{for } t\in(0,\tau), \qquad \text{(B1)}$$

which yields the original analytic solution reported by Schmiedl and Seifert $\lambda^*(t) = \lambda_f(1+t)/(2+\tau)$, Eq. (9) in [19] (note that they use t to denote protocol duration and τ to denote time, which is swapped with respect to our notation). However, we now have a refined interpretation of this optimal protocol, as consisting of a geodesic component that connects λ_i to $\gamma_f \neq \lambda_f$, and a counterdiabatic component necessary to achieve the geodesic trajectory for finite protocol durations τ.

We now solve for the optimal protocol for a variable-stiffness harmonic trap $U_\lambda(x) = \lambda x^2/2$. We will defer solving for γ_f until after obtaining the analytic form for $\lambda^*(t)$. The friction tensor for this potential has previously been shown to be $g(\lambda) = 1/4\lambda^3$ [65], and the Fisher information metric can be calculated to be $h(\lambda) = \langle x^4/4\rangle^{\text{eq}}_\lambda - (\langle x^2/2\rangle^{\text{eq}}_\lambda)^2 = 1/2\lambda^2$. As shown in [65], by switching to standard deviation coordinates $\sigma = \lambda^{-1/2}$, the friction tensor is constant $\tilde{g}(\sigma) = 1$, and thus geodesics are $\sigma(s) = (1-s)\sigma_A + s\sigma_B$ with thermodynamic length $\tilde{\mathcal{T}}^2(\sigma_A,\sigma_B) = (\sigma_B-\sigma_A)^2$, where $\sigma_A = \lambda_i^{-1/2}$ and $\sigma_B = \gamma_f^{-1/2}$. This yields the geodesic

$$\gamma(s) = [(1-s)\sigma_A + s\sigma_B]^{-2}, \qquad \text{(B2)}$$

with the corresponding counterdiabatic term given by

$$\eta(s) = (\sigma_A-\sigma_B)/[(1-s)\sigma_A + s\sigma_B]. \qquad \text{(B3)}$$

Plugging these into $\lambda^*(t) = \gamma(t/\tau) + \tau^{-1}\eta(t/\tau)$ leads to the interpretable optimal protocol expression

$$\lambda^*(t) = \underbrace{[1/\sigma^*(t)]^2}_{\text{geodesic}} + \underbrace{\tau^{-1}[\Delta\sigma/\sigma^*(t)]}_{\text{counterdiabatic}}, \qquad \text{(B4)}$$

where $\sigma^*(t) = \sigma_i + (t/\tau)\Delta\sigma$ is the linear interpolation between the endpoints $\sigma_i = \lambda_i^{-1/2}$ and $\sigma_i + \Delta\sigma = \gamma_f^{-1/2}$.

Finally we solve for γ_f via

$$\gamma_f = \arg\min_{\lambda} \mathcal{T}^2(\lambda_i, \lambda)/\tau + D_{\mathrm{KL}}(\rho_\lambda^{\mathrm{eq}}|\rho_f^{\mathrm{eq}}), \qquad \text{(B5)}$$

using $\mathcal{T}^2(\lambda_i, \lambda) = (\lambda_i^{-1/2} - \lambda^{-1/2})^2$ (recall that $\lambda^{-1/2} = \sigma$ is the standard deviation) and $D_{\mathrm{KL}}(\rho_\lambda^{\mathrm{eq}}|\rho_f^{\mathrm{eq}}) = (1/2)[(\lambda_f/\lambda - 1) + \ln(\lambda/\lambda_f)]$ [94]. This yields

$$\gamma_f = (\sqrt{1 + 2\lambda_i\tau + \lambda_i\lambda_f\tau^2} - 1)^2/\lambda_i\tau^2, \qquad \text{(B6)}$$

or when expressed in σ coordinates

$$\Delta\sigma = \sigma_i \left(\frac{1 + \lambda_f\tau - \sqrt{1 + \lambda_k\tau + \lambda_i\lambda_f\tau^2}}{2 + \lambda_f\tau} \right). \qquad \text{(B7)}$$

Substituting this expression into Eq. (B4) reproduces the exact optimal protocol, Eqs. (18) and (19) in [19]. (Note that they use t to denote protocol duration and τ to denote time, which is swapped with respect to our notation).

Figure 1 illustrates the obtained exact optimal protocol for this problem [Eqs. (B4) and (B7)] as a sum of geodesic and counterdiabatic components. This clarifies the origin of the jumps in optimal protocols: at $t = 0$, the counterdiabatic component is suddenly turned on, and at $t = \tau$ it is abruptly turned off.